Available at https://www.iasj.net/iasj
Iraqi Academic Scientific Journals
Journal homepage:
https://journals.uokerbala.edu.iq/index.php/UOKJ

Research Article

The Effect of Plasma Parameters on the Structural Properties of SiO2/Au Core Shell Nanostructure

[1]Saja H. Al Faddam ,[2] Duaa A. Uamran

[1] Radiology Unit. College of Dentistry, University of Kerbala, Karbala, Iraq

[2] Department of Physics, College of Science, University of Kerbala, Karbala, Iraq

Article Info
Article history:
Received 20 -5-2025
Received in revised form 4-6-2025
Accepted 22-6-2025
Available online 30 -6 -2025
Keywords:
Au plasma, Explosive wire, SiO2, Structural properties, Underwater plasma.

Abstract:

Plasma diagnostics play a pivotal role in understanding plasma behavior and properties in various environments, which enables us to control the plasma parameters required for a suitable application, such as nanoparticle production. In this work, the underwater plasma was generated by exploding gold wires in a SiO_2 suspension. The process is controlled by an Arduino-based system that precisely regulates the circuit, ensuring accurate replication of each pulse. The optical emission spectroscopy (OES) is used to diagnose the plasma simultaneously.

Boltzmann plot was used to calculate the electron temperature, which ranged from **8.374 eV** to **10.321 eV** and the electron density is determined through Stark broadening, which increased from **0.166×10^{18} (cm^{-3}) to 0.449×10^{18} (cm^{-3})**, indicating a direct proportionality between the applied current and the plasma parameters.

The X-ray diffraction (XRD) analysis showed that the nanostructures contained an **FCC** Au structure with crystallite sizes ranging from **12 to 34 nm**.

Corresponding Author E-mail : seja.hameed@s.uokerbala.edu.iq

Peer review under responsibility of Iraqi Academic Scientific Journal and University of Kerbala.

1. Introduction

Pulsed Plasma via arc discharge has attracted the attention of various researchers due to its ability to rapidly focus energy, producing much higher power during each pulse compared to continuously operated plasmas, This makes it a versatile tool for the production of nanomaterials. (Miron C, Zhuang J, Sava I, Kruth A, Weltmann K-D, Kolb JF, 2016) (C. Cornella, S. Portal, D. B. Zolotukhin, L. Martinez, L. Lin, M. N. Kundrapu, and M. Keidar, 2019)

Plasma conventionally operates in a continuous fashion which involves the maintenance of a constant state of ionization, this kind of plasma is mainly used in industrial applications such as welding and surface treatment. (Kim, S., Chung, T., Joh, H., Cha, J., Eom, I., & Lee, H., 2015)

On the other hand, pulsed plasma can be described as a short burst of high energy which is able to create plasma of unique conditions such as high electron temperature and densities with a reduced energy consumption compared to continuous plasma (Lee, S., , S., Hong, Y., & Choi, M., 2018), pulsed plasma is employed in material processing such as nanoparticle production. (Pilch, I., Söderström, D., Brenning, N., & Helmersson, U, 2013)

One of the most attractive pulsed plasma methods utilizes arc discharge is the underwater electrical explosive wire (UEEW) technique, as it is an inexpensive, single-step, and an environment friendly method. (Ali Hashemzadeh, Reza Ahmadi, Davood Yarali and Nafiseh Sanaei, 2019) The UEEW technique consists of sending a high-intensity pulse of electrical current through a thin wire of a conductive material. The passing current causes the wire to melt then vaporize rapidly, and an electric arc through the vapor causes an explosive shock wave which results in the conversion of the wire martial into plasma.

Several factors, including current, voltage, wire dimensions, and the surrounding medium, effect the produced plasma parameters and the nanomaterial properties therefor many researchers attempted to control these factors in order to test their influence, J. Batra et al. compared five different metals (Au, Cu, Al, W, and Ti) in air and vacuum. (J. Batra, A. K. Saxena, A. C. Jaiswar, R. R. Valvi, K. D. Joshi and T. C. Kaushik, 2021), Duaa A. Uamran et al. studied the Core-Shell SiO_2/Ag Composite Spheres Prepared by UEEW technique. (Duaa A. Uamran, Qasim Hassan Ubaid and Hammad R. Humud, 2021), Fathi et al. investigated the plasma parameters for Fe plasma generated by exploding Fe wire in carbon nanotubes-water colloid with three current values (50, 100 and 150) A. (Fathi, Sabah M., and Saba J. Kadhim, 2022) Furthermore, Nawfal A. Laniwai et al. employed the underwater electrical explosion wire (UEEW) method to fabricate core-shell SiO_2 /Ag/Au Nanoparticles. (Alnidawi, Nawfal A., and Saba J. Kadhim, 2021)

A considerable number of studies on plasma generated by the UEEW technique has been conducted experimenting with various metal types and mediums. However limited research exists on plasma generated from the explosion of gold wires underwater, particularly where the UEEW technique is automated.
This work aims to design an Arduino controlled version of the UEEW technique and to analyze the electron temperature and density of Au plasma generated in a solution of SiO_2 via the UEEW technique with three different explosion currents (100, 125, and 150 A) and SiO_2 mass (20, 25, and 30 mg).

2. Experimental Work

2.1 Sample prepration

SiO_2 nanoparticles produced in china by Zhongnuo Advanced Material Technology Co. Ltd. with 99.99% purity and granular size of 30 ± 5nm were quantified using an analytical balance. Three quantities of SiO_2 nanoparticles powder were measured, specifically 20 mg, 25 mg, and 30 mg. Then, each sample was combined with 30 ml of distilled water. From which three distinct

samples were prepared for each mass of SiO_2. The samples were subjected to one of three specified current intensities: 100, 125, and 150 A.

From an alloy of 24K gold, boasting a purity of 99.99%, a cuboid plate measuring 3cm by 2cm and 3mm in thickness and a 12 cm wire with a diameter of 0.3mm were meticulously fabricated to be the electrodes in the UEEW system.

2.2 The underwater exploding wire technique

This technique consists of two electrodes, a metal thin wire and a plate both submerged in a liquid contained in a reaction vessel, the electrical circuit remains open until the thin wire touches the plate which allows the high current to run through the wire causing it to explode underwater. (Shaojie Zhang, Wansheng Chen, Yong Lu, Yongmin Zhang, Shuangming Wang, Aici Qiu, Liang Ma, Liang Gao, and Fei Chen, 2024)

The explosion causes the wire to undergo instant phase transition from solid to plasma which generates a shockwave in liquid, many factors affect the plasma properties such as the wire diameter, the material of the electrodes, the applied current and the underwater medium. (Krasik, Y., Fedotov, A., Sheftman, D., Efimov, S., Sayapin, A., Gurovich, V., Veksler, D., Bazalitski, G., Gleizer, S., Grinenko, A., & Oreshkin, V., 2010)

The electrodynamic force driving the explosions scales with the current squared and can be expressed as:

$$F = I^2 \log {}^{L}/_{D} \ldots\ldots(1)$$

Where I is the current, L is the length of the wire and D is the wire diameter. (H.Aspden, 1985)

The electro-explosion of wires is automated using a Tower Pro MG90S micro servo motor controlled via an Arduino Uno board with the following code:

```
#include <Servo.h>

int servoPin = 11;
Servo servo1;

void setup() {
  servo1.attach(servoPin);
  Serial.begin(9600);
}

void loop() {
  for(int iteration = 0; iteration < 15; iteration++) {
    for(int currentAngle = 90; currentAngle <= 165; currentAngle += 5) {
      servo1.write(currentAngle);
      Serial.print("Iteration: ");
      Serial.print(iteration);
      Serial.print(", Angle: ");
      Serial.println(currentAngle);
      delay(100);
    }
  }
  while(1); // Stop after 15 pulses
}
```

The gold wire is attached to the fan of the motor which moves in a sweeping motion from 90º to 165º with the 5º incement. The precise movements of the motor is achieved via its connection to the coded Arduino board (line 13) which also enables us to achive such short pluse time coded in line 17 which is equivalent to 0.1 second and to be replicated for 30 pulses in line 12 of the code. This provides precise timing and plate-wire contact force control during each wire explosion (pulse) which leads to better reproducibility of plasma conditions and nanoparticle synthesis than manual operation.

Each pulse was recorded via an optical fiber placed in a 45º angel and 3 cm away from the vessel and attached to a spectrometer connected to a computer to display the intensity of the plasma pulses, as shown in Figure 1.

2.3 Thin films preparation

Drop casting is used to prepare a thin film for each sample. A 5 mm pipette was used to drop a determined volume of the liquid samples onto a glass substrate, then allowing the solvent to evaporate at room temperature and repeating the process for 30 drops each until a noticeable thickness was observed.

2.4 X-ray diffraction

The thin film's structure is investigated by an ASENWARE (AW-XDM300) X-ray diffractometer where the radiation source is a Cu (Kα) with a wavelength of 0.154 nm and the current and voltage are 30 mA and 40 kV respectively. The diffraction patterns were reported within a range of 10° to 80° with a 3 degree/min speed.

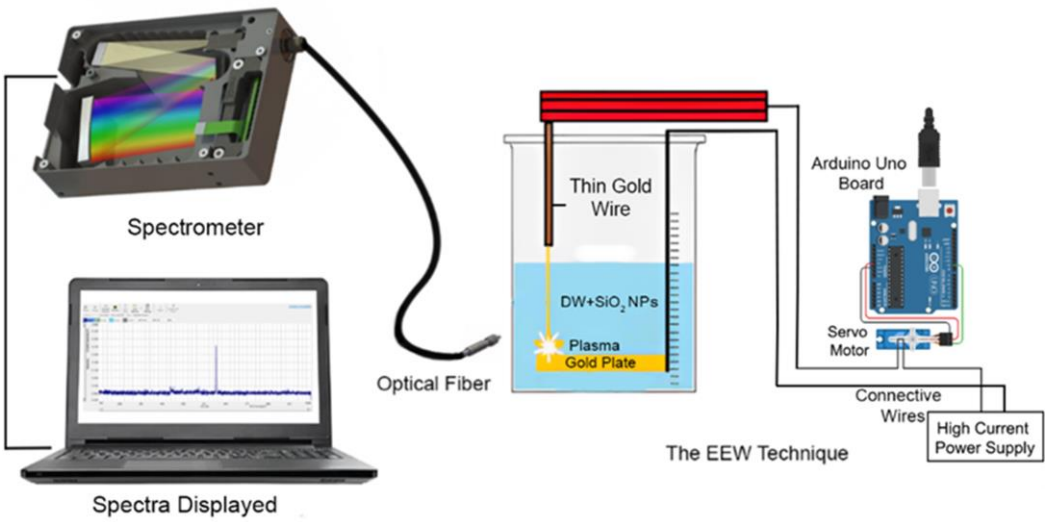

Figure 1: The electrical exploding wire system controlled by Arduino.

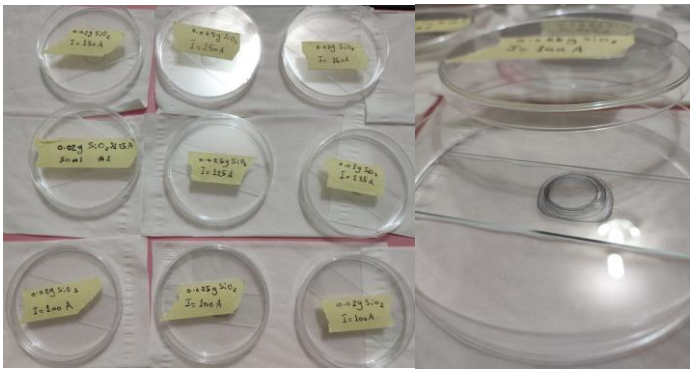

Figure 2: SiO_2/Au Thin Film Preparation.

3. Results and Discussion

3.1 The optical emission spectrum

The emission spectrum of the gold plasma is shown in Figure 3, The spectrum is generated via the electrical explosive wire technique where the wire diameter is only 0.3 mm, the applied currents are 100, 125, and 150 A for the SiO_2 masses of 20, 25, and 30 mg within a wavelength range of (200-800) nm. Each sample spectrum displays a notable singly ionic (II) and atomic (I) lines of (Hα, SiI, SiII, AuI), with a peak detected at 656.28 nm, indicating the Hα line for the hydrogen atoms produced from the dissociation of water molecules as well as AuI peaks for the following wavelengths (385.602, 504.103, 546.643, 566.956, 597.893, 634.71). (J. E. Sansonetti and W. C. Martin, 2005). The difference between the ionic silicon peak and the atomic silicon peak increases linearly with the applied current indicating a higher degree of ionization, which is also evident by the direct proportionality between the intensity of all the present peaks and the applied current. The effect of the added SiO_2 mass was in line with the current.

3.2 Measurements of electron temperature and density

Boltzmann plot is one of the methods used to determine the temperature of electron in case of an equilibrium plasma. Where The wavelength of emitted light depends on energy difference between levels. While the intensity, depends on Boltzmann distribution for local thermal equilibrium and the intensity can be described as: $\ln\left(\frac{\lambda_{ji} I_{ji}}{h_C A_{ji} \cdot g_j}\right) = \frac{-E_j}{k_B T} + C$ (2)

Where: I_{ij}, λ_{ij} and A_{ij} are the intensity, wavelength and transition probability corresponding to transition from i to j, g_j the degeneracy of state j, h is the Planck's constant, K_B is Boltzmann constant, E_j is the energy gap, c is the speed of light, and T_e is the temperature of the electron. (M. Capitelli, G. Colonna, G. D. Ammando, and L. D. Pietanza, 2014)

The AuI spectral lines is to be applied to equation (2) and Table 1 shows the parameters for the AuI wavelenghts taken.

Table 1: shows the AuI wavelenght, itensity , the product of A_{ji}. g_{ij} and the upper-level energy. (NIST Atomic Spectra Database Lines Data)

λ(nm) Observed	Intensity	A_{ji}. g_{ij} (s^{-1})	upper-level E_j (eV)
385.602	0.021478	1.76E+08	10.07388
504.103	0.020844	2.80E+08	12.52526
546.643	0.008	1.30E+08	14.79272
566.956	0.020144	4.00E+08	16.38604
597.893	0.015	2.26E+08	12.14699
634.71	0.019	2.34E+08	10.07388

The relation between the upper energy level (E_j) and the left side of Boltzmann equation $\ln\left(\frac{\lambda_{ji}I_{ji}}{h_C A_{ji}\cdot g_j}\right)$ is represented in Figure 4 for the different values of current and SiO_2 mass. The statistical coefficient (R^2) and the fitting equations are displayed on the figures. The R^2 indicates the priority of the linear fit.

As for the electron density n_e, it can be deduced in many ways, such as Saha-Boltzmann equation or Stark broadening effect is based on the broadening of atomic emission lines due to the electric field effect (Stark effect) caused by the surrounding charged particles (electrons and ions).

$$n_e = \frac{\Delta\lambda_{1/2}}{2w} \times 10^{16} cm^{-3} \qquad (2)$$

Where: w is the electron impact parameter (width per unit electron density, tabulated for different lines) and n_e is the electron density. (Liu, F., Nie, Z., Xu, X., Zhou, Q., Li, L., & Liang, R., 2008) The excitation temperature, Texc, is evaluated from the Boltzmann equation, assuming a Boltzmann distribution of the atomic levels' population. (Zhukov, 2005):

$$ln\left(\frac{I_{ji}\lambda_{ji}}{A_{ji}g_j}\right) = -\frac{E_j}{k_B T_{exc}} + constant \qquad (3)$$

The excitation temperature (T_{exc}) is evaluated from the slope's inverse of the Boltzmann plot ($\ln\left(\frac{I_{ji}\lambda_{ji}}{A_{ji}g_j}\right)$ versus E_j) for the same upper level. (Lesage, 2002)

Figure 5 exhibits the Lorentzian fitting done using Excel for the full width at half maximum in order to determine the electron density, using Stark effect, for the three samples with the different currents and SiO_2 mass depending on the standard values of the broadening of the Hα line. (Toru Sasaki, Yuuri Yano, Mitsuo Nakajima, Tohru Kawamura, and Kazuhiko Horioka, 2006).

The SiO_2 mass impacted the electron temperature and electron density differently where the electron temperature was at its highest when SiO_2 mass was 25 mg, and the lowest T_e corresponded with the 30 mg mass. The electron temperature decline at the 30 mg mass can be explained by the increased concentration of SiO_2 nanoparticles which in turn increase the cooling collisions between the dielectric nanoparticles, analogous to dusty plasma. Meanwhile, the electron density relates directly with the SiO_2 mass, and that is due to the rising concentration of SiO_2 nanoparticles in the medium, which enhance the ionization as evident by the increased peaks intensity from the expiratory nano particle. (D. V. Douanla, Alim, C. G. L. Tiofack, A. Mohamadou, 2021)

It can be noticed that the full-width at half maximum decreases with the decrease of current, which indicates the decrease of the electron density which also agrees with Sabah and Saba results. (Fathi, Sabah M., and Saba J. Kadhim, 2022)

Figure 6 idenitifies the link between electron temperature (Te) and electron density (ne) for the different values of current. The electron temperature Te rises from 8.450 to 9.991 eV for the SiO_2 mass of 20 mg. Similarly, the 25 mg T_e went from 8.837 to 10.321. Finally, the 30 mg T_e ranged from 8.374 to 9.533 and that aligns with Toru Sasaki's et al. results. (Zekun Yin, Jian Wu, Liwen Liang, Chuncai Kong, A. Pervikov, Huantong Shi, Xingwen Li, 2023)

Table 2 shows the plasma parameters such as Debye length (λ_D), plasma frequency (f_p), and Debye number (N_D) for Au plasma in addition to the FWHM of stark broadening. A direct relation exists between the electron temperature\density and the current applied.

(a)

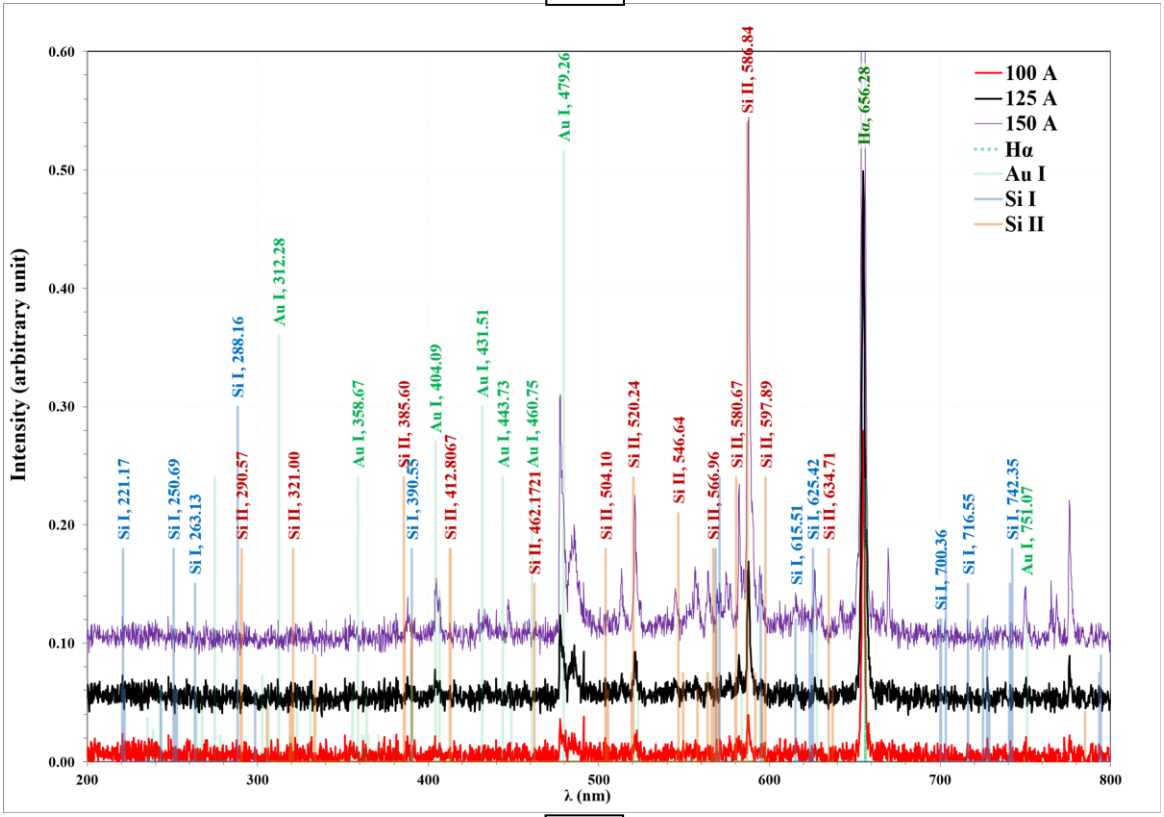
Intensity (arbitrary unit)
λ (nm)
100 A
125 A
150 A
Hα
Au I
Si I
Si II
Si I, 221.17
Si I, 250.69
Si I, 263.13
Si I, 288.16
Si II, 290.57
Au I, 312.28
Si II, 321.00
Au I, 358.67
Si II, 385.60
Si I, 390.55
Au I, 404.09
Si II, 412.8067
Au I, 431.51
Au I, 443.73
Si II, 462.1721
Au I, 460.75
Au I, 479.26
Si II, 504.10
Si II, 520.24
Si II, 546.64
Si II, 566.96
Si II, 580.67
Si II, 586.84
Si II, 597.89
Si I, 615.51
Si I, 625.42
Si II, 634.71
Hα, 656.28
Si I, 700.36
Si I, 716.55
Si I, 742.35
Au I, 751.07

(b)

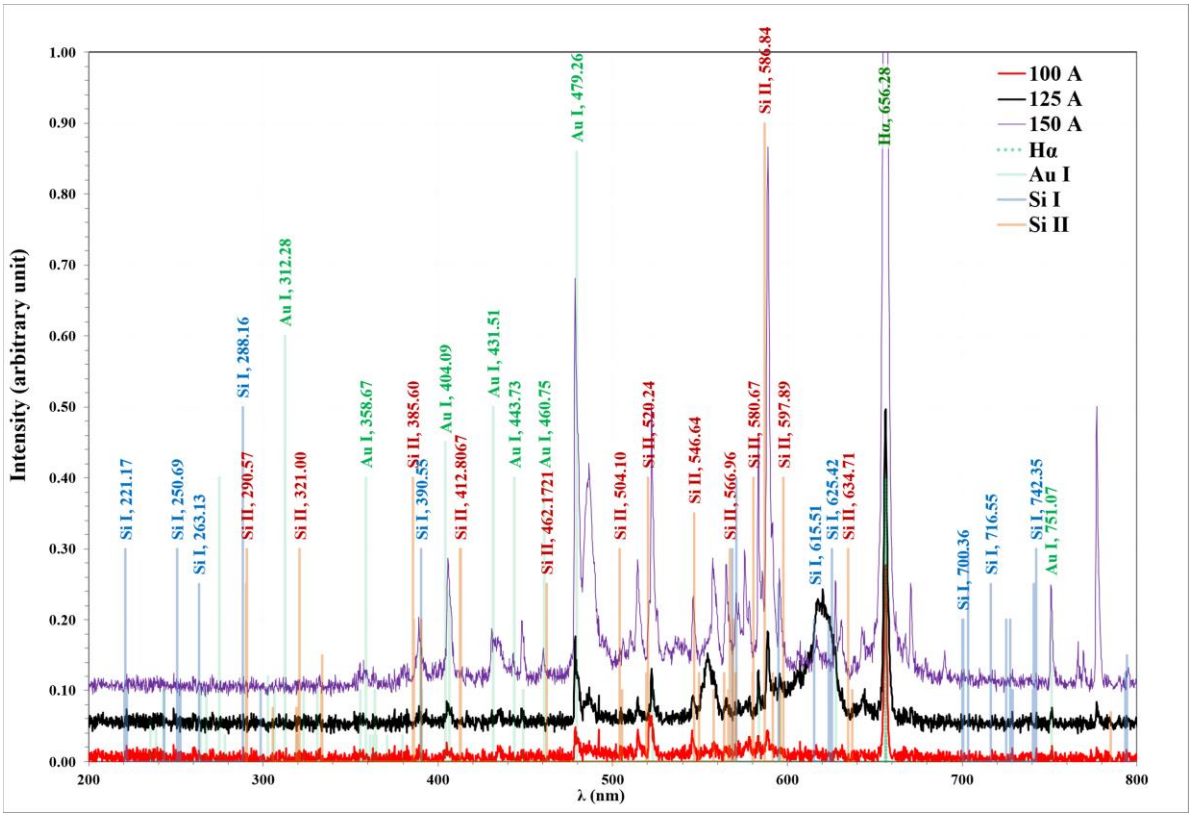
Intensity (arbitrary unit)
λ (nm)
100 A
125 A
150 A
Hα
Au I
Si I
Si II
Si I, 221.17
Si I, 250.69
Si I, 263.13
Si I, 288.16
Si II, 290.57
Au I, 312.28
Si II, 321.00
Au I, 358.67
Si II, 385.60
Si I, 390.55
Au I, 404.09
Si II, 412.8067
Au I, 431.51
Au I, 443.73
Si II, 462.1721
Au I, 460.75
Au I, 479.26
Si II, 504.10
Si II, 520.24
Si II, 546.64
Si II, 566.96
Si II, 580.67
Si II, 586.84
Si II, 597.89
Si I, 615.51
Si I, 625.42
Si II, 634.71
Hα, 656.28
Si I, 700.36
Si I, 716.55
Si I, 742.35
Au I, 751.07

(c)

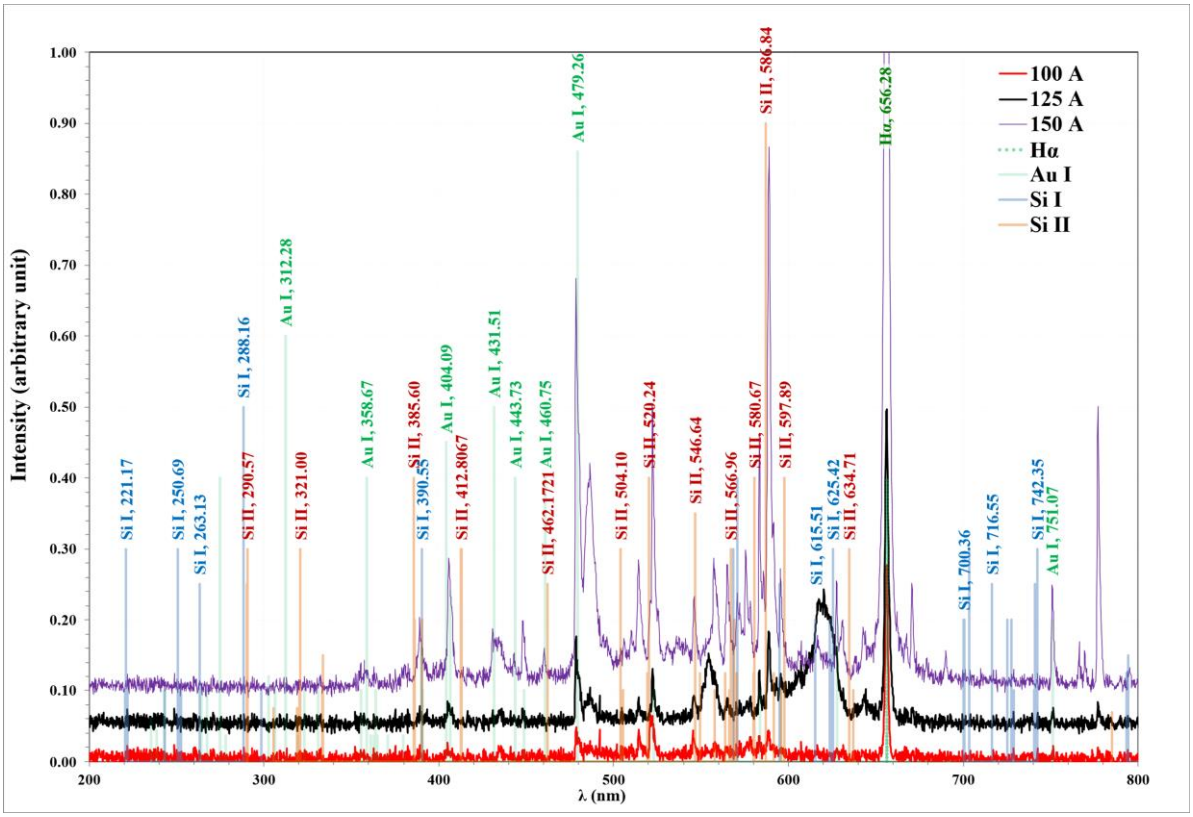

Figure 3: Emission spectra for gold wires with constant SiO_2 mass of a) 20, b) 25, and c) 30 mg and the following currents: 100, 125, and 150 A, obtained by exploding wire.

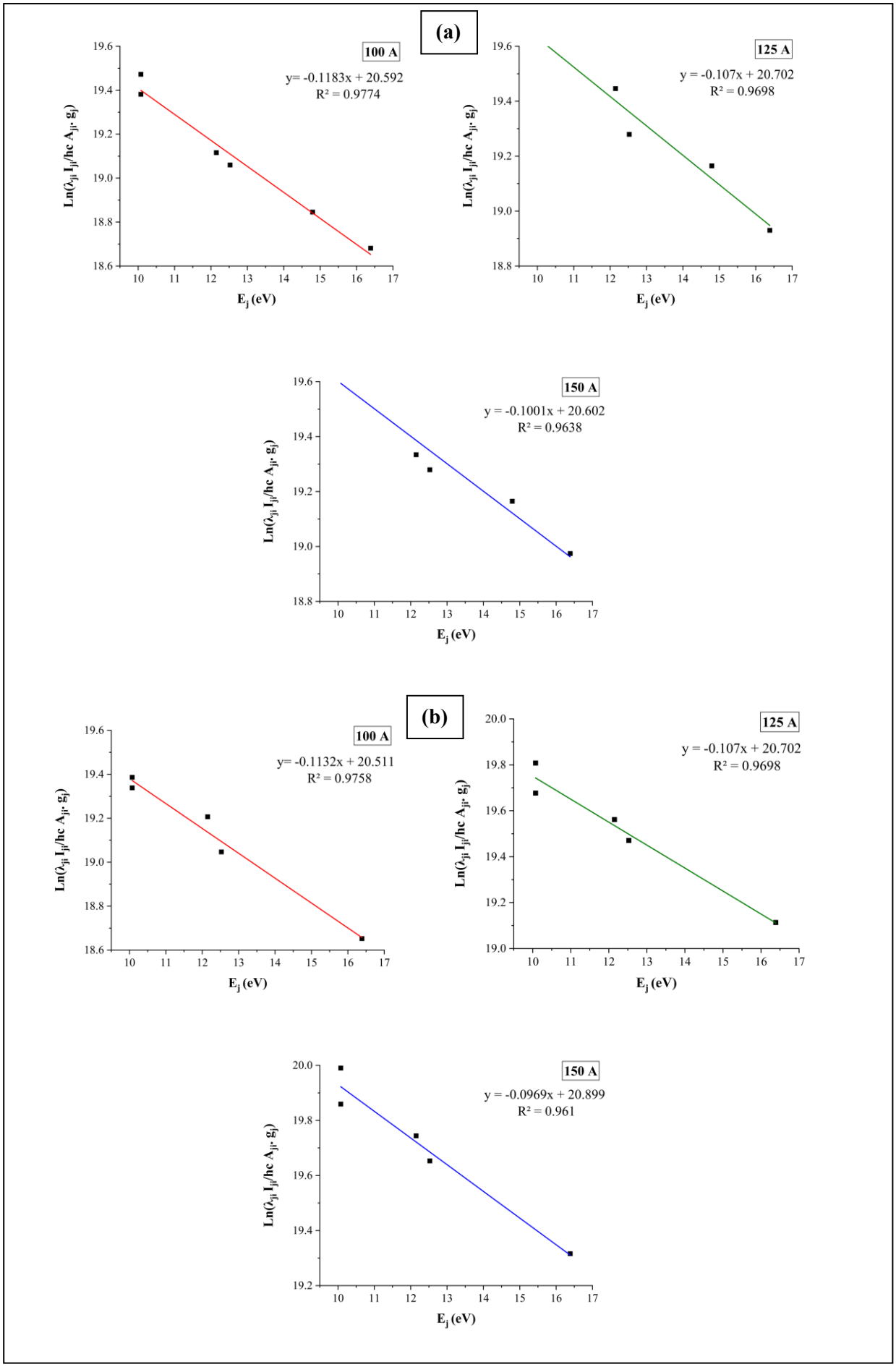
(a)
100 A
y= -0.1183x + 20.592
R² = 0.9774
125 A
y = -0.107x + 20.702
R² = 0.9698
150 A
y = -0.1001x + 20.602
R² = 0.9638
(b)
100 A
y= -0.1132x + 20.511
R² = 0.9758
125 A
y = -0.107x + 20.702
R² = 0.9698
150 A
y = -0.0969x + 20.899
R² = 0.961
Ln(λji Iji/hc Aji. gj)
Ej (eV)

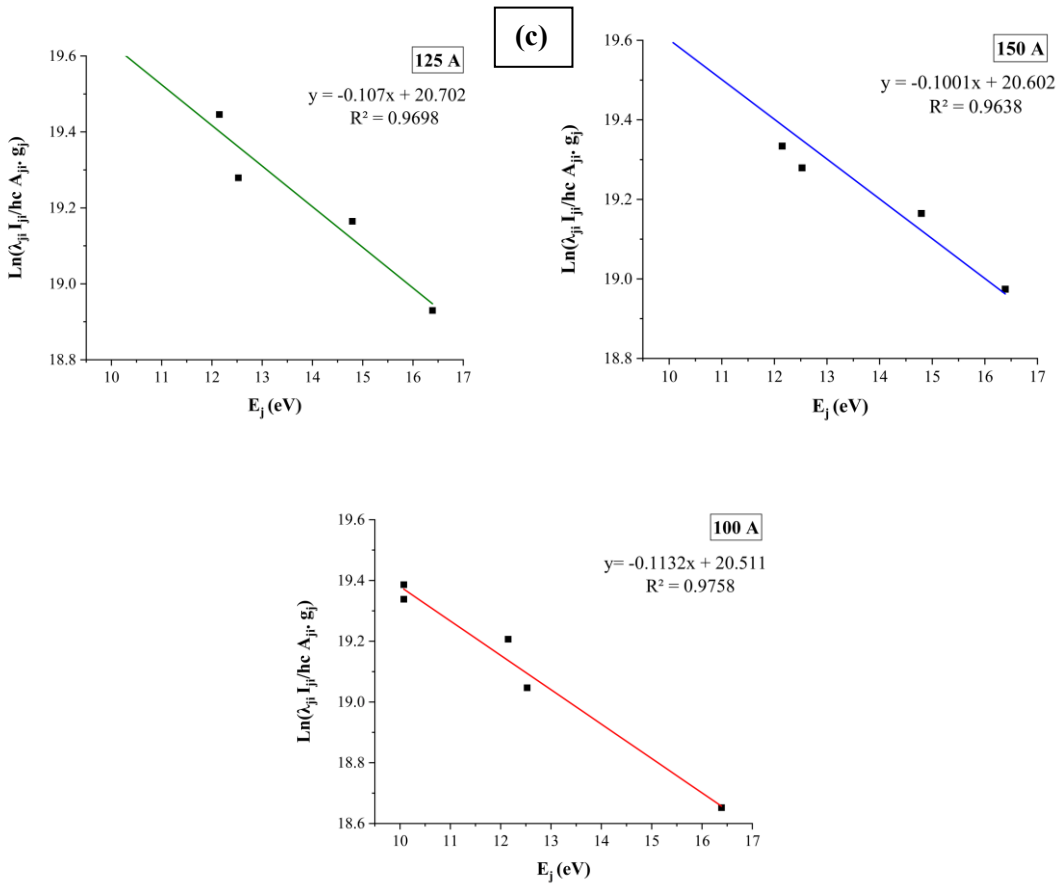

Figure 4: Boltzmann plots for SiO_2/Au lines generated by the explosion of Au wires, where the SiO_2 mass is a) 20, b) 25, and c) 30 mg and the current applied is 100, 125, and

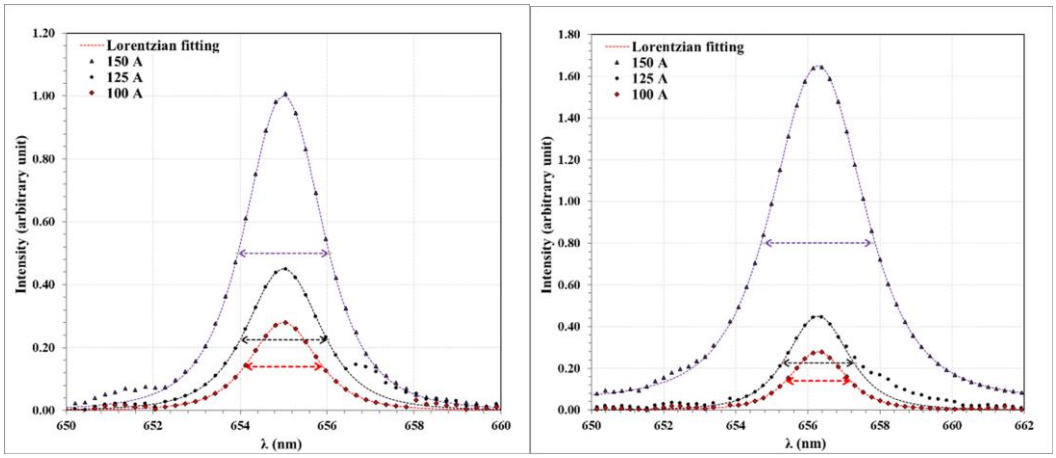

(a) (b)

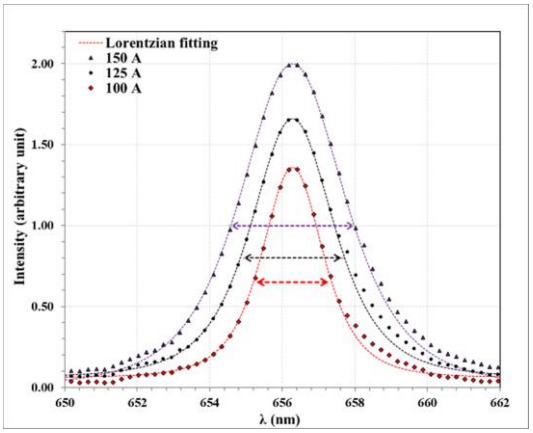

(c)

Figure 5: Shows the peaks broadening and their Lorentzian fitting for (a) 20 mg, (b) 25 mg, and **(c)** 30 mg and currents of (100 ,125 and 150) A.

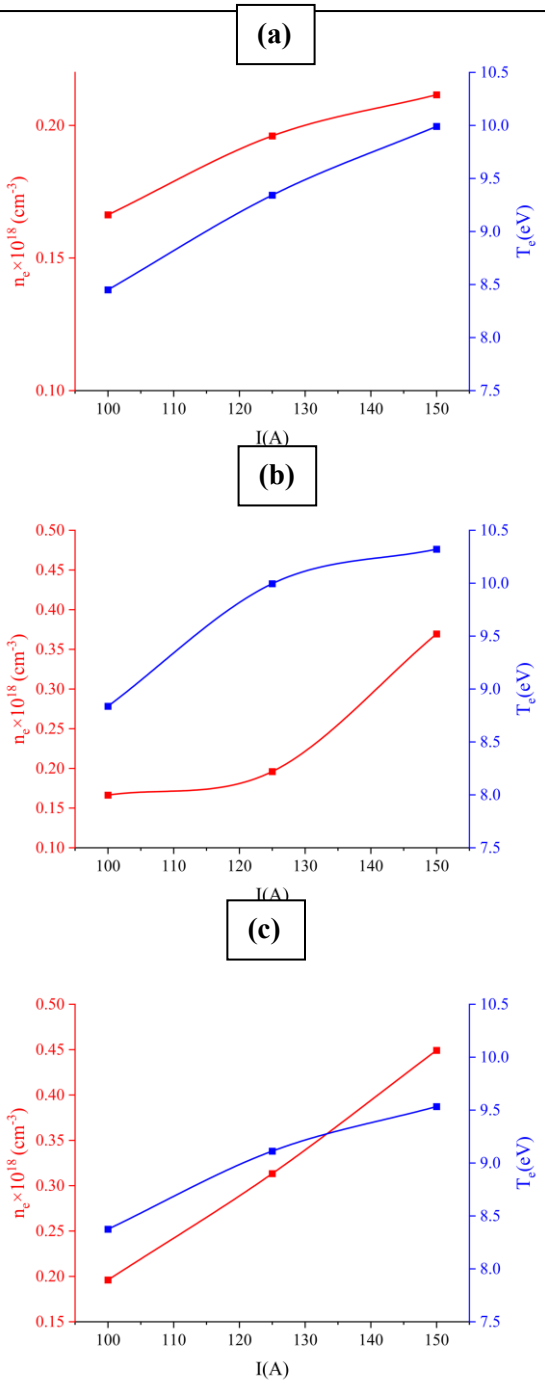

Figure 6: The temperature and density of electrons for the a) 20, b) 25, c) 30 mg SiO_2 mass and currents of 100, 125, and 150 A.

Table 2: Au Plasma parameters of EEW after automation from spectroscopy lines intensity of for (a) 20 mg, (b) 25 mg, and (c) 30 mg of SiO_2 mass and for 100, 125, and 150 A currents.

SiO_2 mass	I(A)	T_e (eV)	$n_e \times 10^{18}$ (cm^{-3})	FWHM (nm)	f_p (Hz) $\times 10^{10}$	$\lambda_D \times 10^{-5}$ (cm)	N_d
20 mg	**100**	8.450	0.166	1.80	366.176	5.297	103496
	125	9.342	0.196	2.00	397.592	5.129	110805
	150	9.991	0.212	2.10	413.040	5.106	117961
25 mg	**100**	8.837	0.166	1.80	366.176	5.417	110683
	125	9.995	0.196	2.00	397.592	5.305	122617
	150	10.321	0.369	3.00	545.769	3.928	93737
30 mg	**100**	8.374	0.196	2.00	397.592	4.856	94039
	125	9.112	0.313	2.70	502.645	4.007	84425
	150	9.533	0.449	3.40	601.833	3.423	75463

3.3 The structural properties

XRD analysis was employed to determine the crystalline phases of the SiO_2/Au samples, the crystalline structures present were identified and calculate the corresponding crystalline parameters.

Figures 7 and 8 show the XRD patterns of the synthesized nanostructures at different SiO_2 concentrations and current values. The XRD pattern includes a cubic gold crystal with a space group of Fm-3m (Davey, 1925) The cubic crystalline structure and the Miller indices of the diffraction peaks are reported in Tables 3 and 4. The crystallite size values were calculated using the Debye-Scherrer equation (F. Hajipour, S. Asad, M.A. Amoozegar, A.A. Javidparvar, J. Tang, H. Zhong, K. Khajeh, 2021).

The analysis of the displayed pattern reveals a diminishing presence of the amorphous SiO_2 curve with the current increase, until it disappears entirely at I = 150 A, the nonlinear relationship between the current and the highest peak of Au (111) is observed in Table 3. The applied current effect may be explained by the enhanced Au shell coverage over the SiO_2 core because of the raised electron temperature, which immediately melts and deposits the Au onto the SiO_2 surface. This is the cause of the increased Au presence on the core, thereby increasing the crystalline size and decreasing the dislocation density.

The SiO_2 mass effect on the XRD pattern is identical to the applied current effect where the Amorphous SiO_2 structure is reduced as the SiO_2 mass increases and that is a result of an increasing number of SiO_2 nanoparticles in the suspension which increases the probability of the Au encapsulation as evident by the higher Au peaks.

The linear relationship between the applied current and the intensity of the Au peaks agrees with the results of Taha M. Rashid, Uday M. Nayef. Majid S. Jabir and Falah A.-H. Mutlak (Taha M. Rashid, Uday M. Nayef. Majid S. Jabir and Falah A.-H. Mutlak, 2021). However, our XRD pattern shows an Au (022) peak, which enhances the plasmonic effect applicable in the surface-enhanced Raman spectroscopy (SERS) (Richa Goel, Sibashish Chakraborty, Vimarsh Awasthi, Vijayant Bhardwaj, Satish Kumar Dubey, 2024; Taha M. Rashid, Uday M. Nayef.

Majid S. Jabir and Falah A.-H. Mutlak, 2021).

Table 3: The crystalline parameters of SiO_2/Au nanostructure, where the SiO_2 mass is 25 mg and the currents are 100, 125, and 150 A.

Current (A)	T_e (eV)	$n_e \times 10^{18}$ (cm^{-3})	2θ	Miller index	FWHM (Radians)	d-spacing (Å)	Height (a.u.)	Crystallite size (nm)	Dislocation Density (nm^{-2})	Phase and Card No.
100	**8.837**	**0.166**	37.90	(111)	0.0113	2.34	48.2	12.915	0.0060	Cubic 96-901-1613
			44.05	(200)	0.0095	2.03	19.0	15.575	0.0041	
			64.25	(220)	0.0087	1.43	4.7	18.779	0.0028	
			77.90	(311)	0.0069	1.21	3.5	25.501	0.0015	
125	**9.995**	**0.196**	37.70	(111)	0.0108	2.34	42.3	13.538	0.0055	
			44.05	(200)	0.0095	2.03	12.0	15.575	0.0041	
			64.25	(220)	0.0095	1.43	3.4	17.072	0.0034	
			78.10	(311)	0.0052	1.21	2.9	34.085	0.0009	
150	**10.321**	**0.369**	38.00	(111)	0.0104	2.34	65.3	13.995	0.0051	
			44.05	(200)	0.0087	2.03	23.1	17.132	0.0034	
			64.50	(220)	0.0087	1.43	5.3	18.779	0.0028	
			77.80	(311)	0.0087	1.21	10.7	20.400	0.0024	

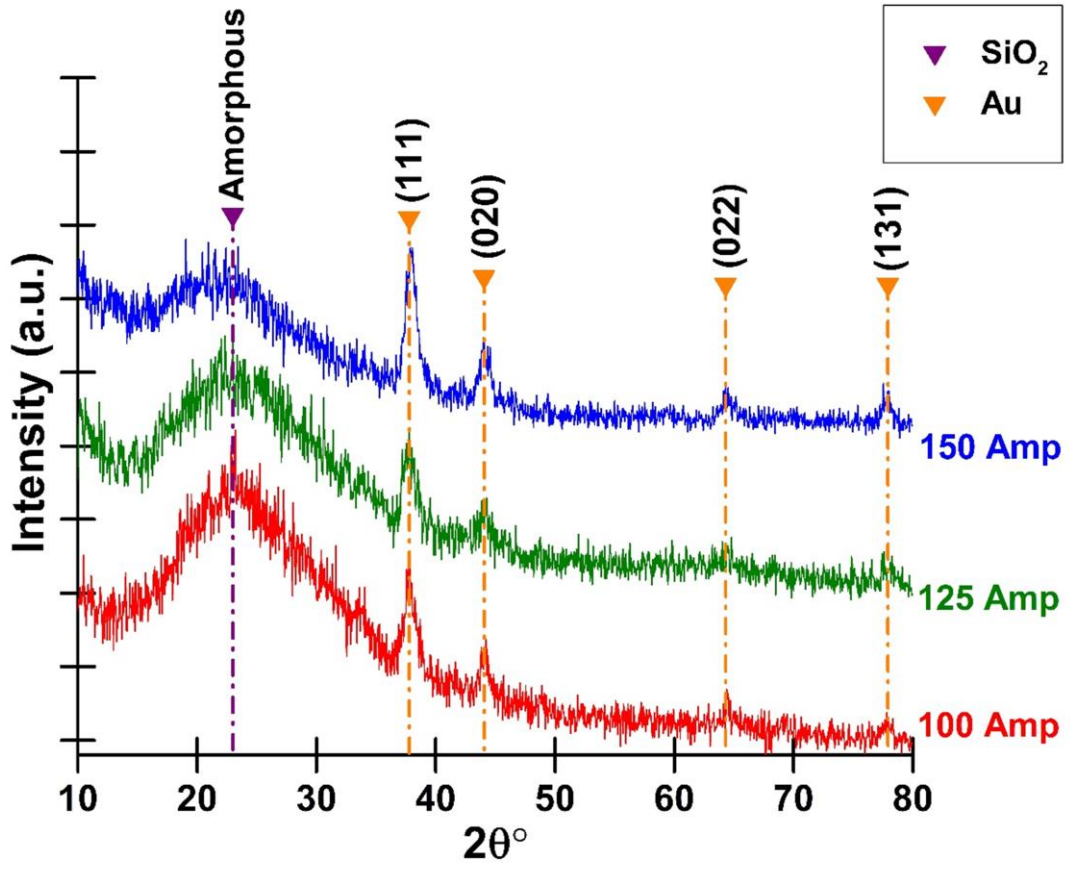

Figure 7: X-ray diffraction of SiO_2/Au nanostructure with a SiO_2 mass of 25 mg and currents of 100, 125, and 150 A.

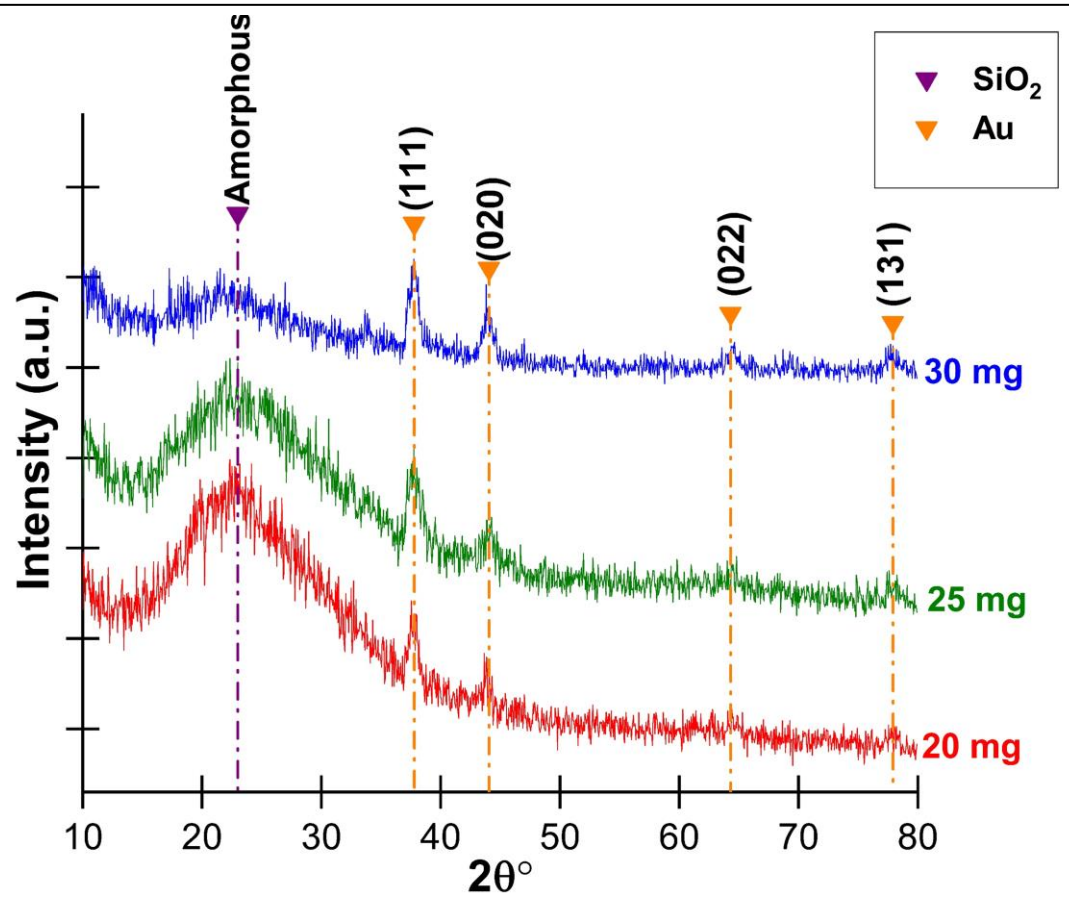

Figure 8: X-ray diffraction of SiO_2/Au nanostructure with an applied current of 125 A and SiO_2 mass of 20, 25, and 30 mg.

Table 4: The crystalline parameters of SiO_2/Au nanostructure, where the applied current is 125 A and the SiO_2 mass of 20, 25, and 30 mg.

SiO_2 Mass (mg)	T_e (eV)	$n_e \times 10^{18}$ (cm^{-3})	2θ	Miller index	FWHM (Radians)	d-spacing (Å)	Height (a.u.)	Crystallite size (nm)	Dislocation Density (nm^{-2})	Phase and Card No.
20	**9.342**	**0.196**	37.80	(111)	0.0096	2.34	31.5	15.261	0.0043	Cubic 96-901-1613
			44.05	(200)	0.0091	2.03	13.0	16.473	0.0037	
			64.30	(220)	0.0073	1.43	5.1	22.332	0.0020	
			78.10	(311)	0.0070	1.21	3.5	25.564	0.0015	
25	**9.995**	**0.196**	37.80	(111)	0.0105	2.34	42.3	13.989	0.0051	
			43.80	(200)	0.0087	2.03	6.0	17.118	0.0034	
			64.40	(220)	0.0096	1.43	3.4	17.062	0.0034	
			78.10	(311)	0.0052	1.21	2.8	34.085	0.0008	
30	**9.112**	**0.313**	37.72	(111)	0.0093	2.34	62.0	15.833	0.0039	
			43.80	(200)	0.0101	2.03	19.0	14.756	0.0045	
			64.40	(220)	0.0087	1.43	5.2	18.769	0.0028	
			77.75	(311)	0.0084	1.21	3.3	21.250	0.0022	

Tables 3 and 4 both show how the structural properties relate to the plasma parameters where an inverse relationship is noticeable between the electron density n_e and the declining SiO_2 amorphous presence in the samples in addition to a linear proportionality with the dislocation density. Both are evidence of fewer defects and improved SiO_2\Au core-shell interface. This is due to the increased collation rate and localized heating. While the T_e relation with the structural properties is not linear.

4. Conclusion

The electrical exploding wire (UEEW) technique enabled the successful production and characterization of SiO□/Au core-shell nanostructures within a SiO_2 suspension. The investigation employed optical emission spectroscopy (OES) to investigate the plasma parameters.

The electron temperature (T_e) and electron density (n_e) measurements used Boltzmann plots (Figure 4) and Stark broadening (Figure 5) to determine these values. The linear relationship between Te and ne measurements increased with current strength until Te reached its peak at 25 mg SiO□ during optimal plasma conditions.

XRD analysis confirmed the FCC structure (Fm-3m) of Au, with crystallite dimensions calculated using the Debye-Scherrer equation (Figures. 7 & 8). The Au (111) peak intensity increased with higher currents, improving deposition, while the (220) peak suggests enhanced plasmonic applications like SERS. Plasma parameters (Te and ne) influenced nanostructure crystallinity, with higher ne reducing amorphous SiO□ and defects in SiO□/Au core-shell structures. However, Te and ne affected crystalline size inconsistently,

with Te showing random variations. These results demonstrate the interplay between plasma conditions and the nanostructure properties.

The properties of the produced SiO□/Au nanostructures can be controlled through variations of current and SiO□ weight to adjust their properties to fit various applications such as Photocatalysis, Solar energy harvesting, and SERS and optical devices.

Conflict of Interests

The authors declare no conflict of interest regarding this manuscript.

Acknowledgments

I would like to express my gratitude to the staff of the Physics Department – College of Science at the University of Kerbala for their assistance in accessing numerous resources necessary for this project.

References

[1] Miron C, Zhuang J, Sava I, Kruth A, Weltmann K-D, Kolb JF, "Dielectric spectroscopy of polyimide films treated by nanosecond high voltage pulsed driven electrical discharges in water," *Plasma Processes and Polymers,* vol. 13, no. 2, p. 253–257, 2016.

[2]C. Cornella, S. Portal, D. B. Zolotukhin, L. Martinez, L. Lin, M. N. Kundrapu, and M. Keidar, "Pulsed anodic arc discharge for the synthesis of carbon nanomaterials," *Plasma Sources Sci,* vol. 28, no. 4, p. 045016, 2019.

[3]Kim, S., Chung, T., Joh, H., Cha, J., Eom, I., & Lee, H., "Characteristics of Multiple Plasma Plumes and Formation of Bullets in an Atmospheric- Pressure Plasma Jet Array," *IEEE Transactions on Plasma Science,* vol. 43, pp. 753-759, 2015.

[4]Lee, S., S., Hong, Y., & Choi, M., "Effects of pulsed and continuous wave discharges of underwater plasma on Escherichia coli.," *Separation and Purification Technology,* vol. 193, pp. 351-357, 2018.

[5]Pilch, I., Söderström, D., Brenning, N., & Helmersson, U, "Size-controlled growth of nanoparticles in a highly ionized pulsed plasma," *Applied Physics Letters,* vol. 102, p. 033108, 2013.

[6]Ali Hashemzadeh, Reza Ahmadi, Davood Yarali and Nafiseh Sanaei, "Synthesis of MO2 nanoparticles via the electro-explosion of wire (EEW) method," *Mater. Res. Express,* vol. 6, no. 12, 2019.

[7]J. Batra, A. K. Saxena, A. C. Jaiswar, R. R. Valvi, K. D. Joshi and T. C. Kaushik, "Experimental Study on Electrical Explosion Behavior of Six Metal Wires in Air and Vacuum," *IEEE Transactions on Plasma Science,* vol. 49, no. 9, pp. 2866-2877, 2021.

[8]Duaa A. Uamran, Qasim Hassan Ubaid and Hammad R. Humud, "Core-Shell SiO2/Ag Composite Spheres Prepared by Electrical Exploding Wire Plasma Technique: Synthesis and Characterization," *NeuroQuantology,* vol. 19, no. 10, pp. 82-88, 2021.

[9]Fathi, Sabah M., and Saba J. Kadhim, "Optical Emission Spectroscopy for Studying Fe Plasma Parameters Produced by Exploding Wire Technique in Carbon Nanotubes-Water Colloid," *Iraqi Journal of Science,* vol. 63, no. 1, pp. 163-169, 2022.

[10]Alnidawi, Nawfal A., and Saba J. Kadhim, "Synthesis and characterizations of core-shell SiO2/Au/Ag nanoparticles by exploding of wire and pulsed laser plasmas," *AIP Conference Proceedings,* vol. 2372, no. 1, 2021.

[11]Shaojie Zhang, Wansheng Chen, Yong Lu, Yongmin Zhang, Shuangming Wang, Aici Qiu, Liang Ma, Liang Gao, and Fei Chen, "Underwater electrical wire explosions under different discharge types: An experimental study with high initial energy storage," *Physics of Plasmas,* vol. 3, no. 4, 2024.

[12]Krasik, Y., Fedotov, A., Sheftman, D., Efimov, S., Sayapin, A., Gurovich, V., Veksler, D., Bazalitski, G., Gleizer, S., Grinenko, A., & Oreshkin, V., "Underwater electrical wire explosion," *Plasma Sources Science and Technology,* vol. 19, p. 034020, 2010.

[13] H.Aspden,"The exploding wire phenomenon," *Physics Letters A,* vol. 107, no. 5, pp. 238-240, 1985.

[14]J. E. Sansonetti and W. C. Martin, "Handbook of Basic Atomic Spectroscopic Data," *Am. Inst. Phys,* vol. 34, no. 4, pp. 1739-2001, 2005.

[15]M. Capitelli, G. Colonna, G. D. Ammando, and L. D. Pietanza, Laser-Induced Breakdown Spectroscopy, Berlin Heidelberg: Springer Series in Optical Sciences, 2014.

[16]"NIST Atomic Spectra Database Lines Data," [Online]. Available:https://physics.nist.gov/cgibin/ASD/lines1.pl?spectra=Au+I&output_type=0&low_w=&upp_w=&unit=1&submit=Retrieve+Data&de=0&plot_out=0&I_scale_type=1&format=0&line_out=0&en_unit=0&output=0&bibrefs=1&page_size=15&show_obs_wl=1&show_calc_wl=1&unc_out=1&order_o.

[17]Liu, F., Nie, Z., Xu, X., Zhou, Q., Li, L., & Liang, R., "Measurement of electron density by Stark broadening in an ablative pulsed plasma thruster," *Applied Physics Letters,* vol. 93, p. 111502, 2008.

[18]M. Zhukov, Plasma Diagnostics, Mosco: Cambridge International Science Publishing, 2005.

[19]A. Lesage, "Experimental Stark Widths and Shifts for Spectral Lines of Neutral and Ionized Atoms," *J. Phys. Chem,* vol. 31, no. 3, pp. 819-972, 2002.

[20]Toru Sasaki, Yuuri Yano, Mitsuo Nakajima, Tohru Kawamura, and Kazuhiko Horioka, "Warm-dense-matter studies using pulse-powered wire discharges in water," *Laser and Particle Beam,* vol. 24, no. 1-2, pp. 371-380, 2006.

[21]D. V. Douanla, Alim, C. G. L. Tiofack, A. Mohamadou, Dust–Acoustic Envelope Solitons and Rogue Waves in a Magnetized Electron-Depleted Plasma, vol. 47, Plasma Physics Reports, 2021, p. 384–395.

[22]Zekun Yin, Jian Wu, Liwen Liang, Chuncai Kong, A. Pervikov, Huantong Shi, Xingwen Li, "Microwave-absorbing performance of FeCoNi magnetic nanopowders synthesized by electrical explosion of wires," *Journal of Alloys and Compounds,* vol. 966, no. 171594, 2023.

[23]W. Davey, "The Lattice Parameter And Density Of Pure," *Physical Review,* vol. 25, pp. 753-761, 1925.

[24]F. Hajipour, S. Asad, M.A. Amoozegar, A.A. Javidparvar, J. Tang, H. Zhong, K. Khajeh, "Developing a fluorescent hybrid Nanobiosensor Based on Quantum Dots and Azoreductase Enzyme Formethyl Red Monitoring," *Iran Biomed,* vol. 25, 2021.

[25]Taha M. Rashid, Uday M. Nayef. Majid S. Jabir and Falah A.-H. Mutlak, "Synthesis and characterization of Au: ZnO (core: shell)," *Optik,* vol. 244, p. 167569, 2021.

[26]Richa Goel, Sibashish Chakraborty, Vimarsh Awasthi, Vijayant Bhardwaj, Satish Kumar Dubey, "Exploring the various aspects of Surface-enhanced Raman spectroscopy (SERS) with focus on the recent progress: SERS-active substrate, SERS-instrumentation, SERS-application," *Sensors and Actuators A: Physical,* vol. 376, 2024.